Accepted Manuscript online: 2021-06-22 Article published online: 2021-08-25

Structure–Assembly–Property Relationships of Simple Ditopic Hydrogen-Bonding-Capable π-Conjugated Oligomers

Asmerom O. Weldeab[a]
Cory T. Kornman[a]
Lei Li[a,b]
Daken J. Starkenburg[c]
Xueying Zhao[c]
Danielle E. Fagnani[a]
Sara J. Sadovy[c]
Scott S. Perry[c]
Jiangeng Xue*[c]
Ronald K. Castellano*[a]

[a] Department of Chemistry, University of Florida, PO Box 117200, Gainesville, FL, 32611, United States
[b] Department of Materials Science and Engineering, Clemson University, Clemson, SC, 29634, United States
[c] Department of Materials Science and Engineering, University of Florida, PO Box 116400, Gainesville, FL, 32611, United States
castellano@chem.ufl.edu; jxue@mse.ufl.edu

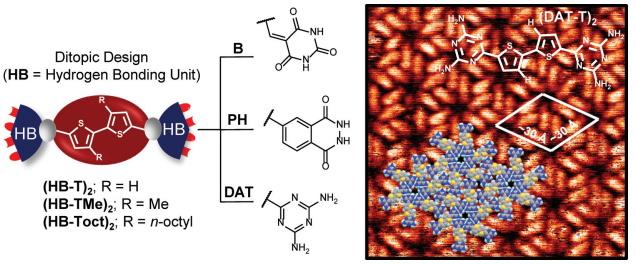

Received: 24.05.2021
Accepted after revision: 17.06.2021
DOI: 10.1055/a-1534-1508; Art ID: om-21-0034oa

Abstract A series of simple ditopic hydrogen-bonding-capable molecules functionalized with 2,4-diamino-1,3,5-triazine (DAT), barbiturate (B), and phthalhydrazide (PH) on both termini of a 2,2′-bithiophene linker were designed and synthesized. The intrinsic electronic structures of the ditopic DAT, PH, and B molecules were investigated with ground-state density functional theory calculations. Their solution absorbance was investigated with UV-vis, where it was found that increasing size of R group substituents on the bithiophene linker resulted in a general blue-shift in solution absorbance maximum. The solid-state optical properties of ditopic DAT and B thin films were evaluated by UV-vis, and it was found that the solid-state absorbance was red-shifted with respect to solution absorbance in all cases. The three DAT molecules were vacuum-thermal-deposited onto Au(111) substrates and the morphologies were examined using scanning tunneling microscopy. **(DAT-T)$_2$** was observed to organize into six-membered rosettes on the surface, whereas **(DAT-TMe)$_2$** formed linear assemblies before and after thermal annealing. For **(DAT-Toct)$_2$**, an irregular arrangement was observed, while **(B-TMe)$_2$** showed several co-existent assembly patterns. The work presented here provides fundamental molecular–supramolecular relationships useful for semiconductive materials design based on ditopic hydrogen-bonding-capable building blocks.

Key words conjugated molecules, hydrogen bonding, organic monolayers, optoelectronic properties, self-assembly, supramolecular chemistry

Introduction

Organic semiconductors are widely accepted as promising candidates for the development of next-generation electronic and optoelectronic devices.[1–4] These π-conjugated organic materials display many attractive features and are capable of being fabricated into light-weight and flexible devices at lower cost than traditional silicon-based semiconductors.[1–3,5] The optoelectronic and physical properties of organic materials largely depend on the structural geometry and electronic structure of the constituent molecules, and significant advancements have been made towards predicting and tuning these properties from a computational and synthetic perspective.[6,7] However, the arrangement and packing of molecules in the solid state is a crucial aspect affecting overall functional performance, and it is recognized that controlling solid-state bulk organization still remains a great challenge.[8–16] Several post-synthetic approaches have been investigated to control solid-state packing, including thermal and solvent annealing techniques and the addition of functional additives to promote a desired architecture.[17–20] Alternatively, a supramolecular approach is a promising and reliable method in which directing groups that induce self-assembly can be introduced at the molecular level during synthesis to guide and control the formation of an ordered system.[21,22] Our group and others have explored hydrogen bonding (HB) in this context using organic photovoltaic (OPV) and organic field-effect transistor testbeds to probe the effects of HB-induced assembly on morphology and device performance.[23–28] Our interest in HB units extends from our attempts to program bulk heterojunction photovoltaic active layer structures in vacuum-deposited films.[29–31]

We have gravitated towards rosette-forming HB units because our earlier work showed these can confer columnar supramolecular architectures upon π-stacking that facilitate charge transport and blend well with fullerenes in the context of bulk heterojunction OPV active layers.[24,32] Our initial studies focused on "monotopic" designs, wherein a HB-capable unit was appended on only one terminus of a mostly linear π-conjugated system (Figure 1a). For our previous work, linear and branched oligothiophene backbones functionalized with a HB-capable phthalhydrazide (PH) unit were fabricated into OPV devices, and their power conversion efficiencies were found to be two-fold higher relative to HB-incapable comparator molecules with similar intrinsic properties.[25] The self-assembly aspects were studied by scanning tunneling microscopy (STM) on monolayers deposited on Au(111) surfaces,[26] where it was observed that the compounds functionalized with PH units formed HB-induced trimeric rosettes with good packing ordering within the monolayer. These could further stack vertically through π–π interactions based on characterizations in solution and in thin films.

In contrast to monotopic targets, one might envision that "ditopic" designs could potentially lead to infinite networks, upon which, controlled stacking interactions could result in long-range ordered covalent/non-covalent superstructures reminiscent of covalent organic frameworks (COFs),[33] or hydrogen-bonded organic frameworks (HOFs).[34] Before exploring this concept in the context of ordered active layers in a semiconducting device, which is a general future direction of this work, presented here are synthesis, processing, and intrinsic characterization of simple families of "ditopic" targets, wherein HB-capable units are pre-installed on both termini of a small π-conjugated chromophore (Figure 1b).

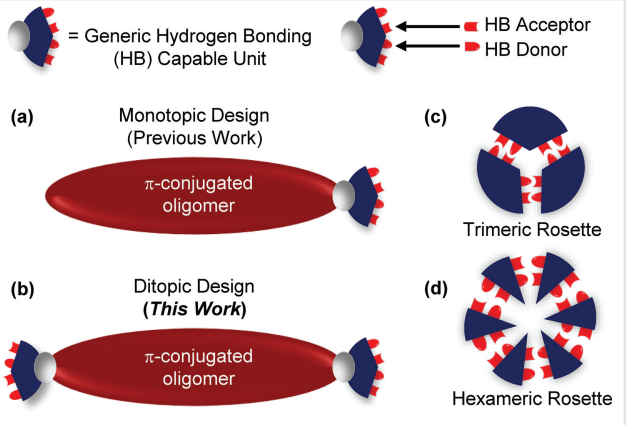

Figure 1 Schematic representations of (a) monotopic and (b) ditopic designs where the H-bonding unit is appended to either one or both ends of a π-conjugated chromophore. Generic representation of (c) HB-induced trimeric rosette, and (d) HB-induced hexameric rosette.

The HB-capable units selected for this study are 2,4-diamino-1,3,5-triazine (DAT), barbiturate (B), and phthalhydrazide (PH). The DAT group is a triazine-based heterocycle with HB-capable functionality. Molecules functionalized with the DAT moiety are well understood, largely thanks to the pioneering work of Wuest et al.[35–37] The self-assembly of monotopic DAT species has been studied in solution, in the solid state, and at solid–liquid interfaces revealing a HB-induced cyclic hexamer as the most prevalent HB-based arrangement (Figure 2a).[37–41] Barbiturate (B) is a HB-capable heterocycle with a structure based on pyrimidine (Figure 2b). The cyclic core is decorated with three alternating carbonyls interspaced with two amine functionalities enabling this unit to engage in HB-directed assembly. Seminal work by Yagai et al. has shown the barbiturate unit can be employed to guide the assembly of various nanostructures such as rods, rings, coils, and catenanes.[42–45] In addition, the HB-induced arrangement of a monotopic π-conjugated system featuring a barbiturate

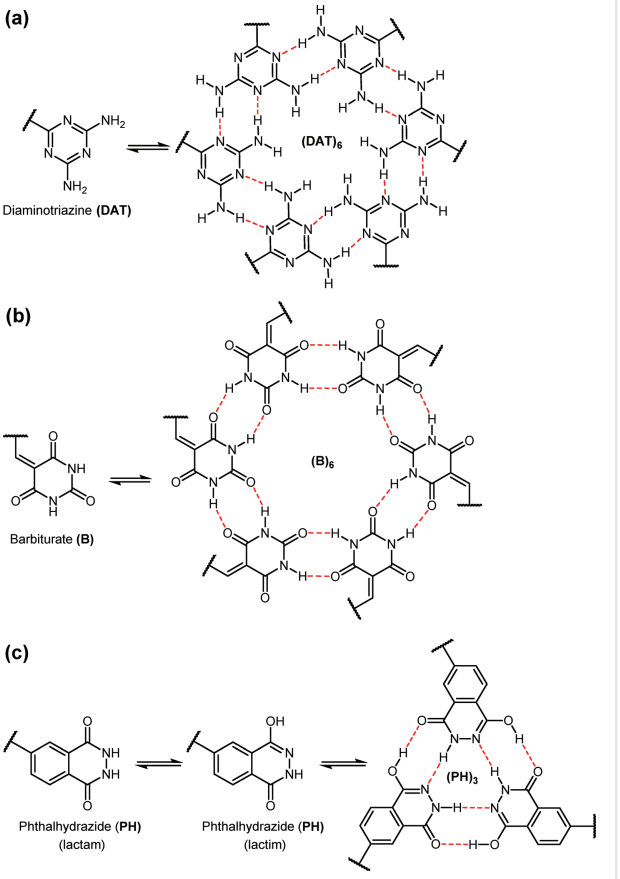

Figure 2 Chemical structures of (a) 2,4-diamino-1,3,5-triazine (DAT) and the HB-induced hexameric rosette $(DAT)_6$, (b) barbiturate (B) unit and the HB-induced hexameric rosette $(B)_6$, and (c) phthalhydrazide (PH) lactam–lactim tautomerization to yield trimeric rosette formation $(PH)_3$. In all cases, dashed lines represent HB-bonding interactions. All rosettes are depicted in the most symmetrical form.

unit was studied by STM.[46] Similar to previous work done on DAT derivatives, barbiturate systems have also been demonstrated to form HB-induced hexameric rosettes at the solid–liquid interface.[23,46,47] Phthalhydrazide (PH) is a HB unit which has been shown to form trimeric rosettes by means of lactam–lactim tautomerization in the solid state and at the solid–liquid interface.[48–50] The lactim tautomer bears a carbonyl HB acceptor and acidic hydrogens bonded to the amide and enol HB donor groups. The lactim tautomeric form enables specific HB interactions to yield trimeric rosette formation (Figure 2c).

Herein, we report the design, synthesis, and characterization of a homologous library of π-conjugated ditopic systems based on DAT, B, and PH HB-capable units (Figure 3). These designs include a varying series of bithiophenes to serve as the π-conjugated linker, which were modified with different R group substituents on the bithiophene unit (R = H, Me, *n*-octyl). The steric and electronic effects of R group substitution on the molecular conformation, photophysical properties, and HB-directed assembly of each species were investigated. The photophysical properties of the various targets were investigated in solution by UV-vis spectroscopy and Beer–Lambert analysis to assess the degree of aggregation within a selected concentration range. The thermal stability of all DAT, B, and PH derivatives were analyzed by thermogravimetric analysis (TGA). Theoretical investigations were done in the gas phase for DAT, B, and PH structures by ground-state density functional theory (DFT) simulations, both at true minima and local minima located through optimization of structures forced into planarization by means of redundant coordinate constraints to mimic packing in the solid-state environment. Vacuum thermal evaporation conditions were optimized for the DAT and barbiturate derivatives and post-deposition structural integrity was analyzed for representative substrates by ^{1}H NMR analysis. The solid-state absorption of thin films revealed a red-shifted optical response compared to the corresponding solution absorbance, speaking to the enhanced planarity, and packing of the molecules in the solid state. The DAT compounds were amenable to deposition onto Au(111) substrates under ultrahigh vacuum (UHV) conditions, and the resulting supramolecular assemblies were studied by STM, where the observed assemblies of the DAT family highlights the delicate interplay between favorable non-covalent interactions and energetically disfavored inter- and intramolecular steric interactions that drive the assembly and manifest in the resultant morphologies.

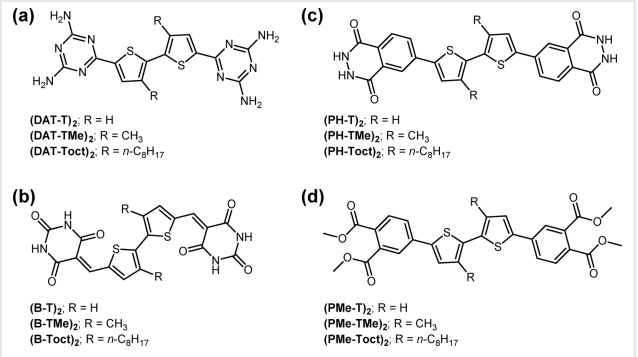

Figure 3 Molecular representations of the simple ditopic systems studied in this work based on (a) diaminotriazine (DAT), (b) barbiturate (B), and (c) phthalhydrazide HB-capable units (PH), and (d) phthalic ester HB-incapable units (PMe).

Results and Discussion

The syntheses of all intermediates and final targets are shown in Schemes S1–S3 in the Supporting Information. Intermediates **1**, **3**, and **8** were synthesized following literature procedures.[51,52] Intermediates **2**, **4**, and **9**, although reported in the literature,[53–55] were synthesized following modified routes. For the synthesis of PH targets, intermediates **12** and **14** were synthesized following literature procedures, with modifications.[24,53,56] When possible, the structural integrity of all reported compounds were confirmed by ^{1}H and ^{13}C NMR (see pages S7–S28, Supporting Information) and high-resolution mass spectrometry (HRMS). However, attempts to perform ^{13}C NMR for **(PH-T)$_2$**, **(PH-TMe)$_2$**, **(B-T)$_2$**, and **(B-TMe)$_2$** were not successful due to their poor solubility, and only ^{1}H NMR and HRMS characterization were performed to confirm these structures. When relevant, the ^{1}H NMR data for the synthesized intermediates matched the literature-reported values (see Experimental Section).

The intrinsic properties of the DAT, B, and PH derivatives were studied at the molecular level in solution (UV-vis) and in the gas phase by ground-state DFT calculations. The solution absorbance and DFT results (vide infra) are summarized in Table 1. The UV-vis absorbance experiments were recorded in DMSO for all final targets. Each DAT compound displays a single absorption band in the UV region which speaks to the wide optical gap of these substrates (Figure 4a), an observation which was also confirmed by DFT (Table 1). The non-alkylated derivative, **(DAT-T)$_2$**, shows the most red-shifted absorption maximum (λ_{max} = 378 nm). A 35 nm blue-shift in λ_{max} was observed upon installation of methyl groups onto the bithiophene linker, resulting in the λ_{max} for **(DAT-TMe)$_2$** residing closer to 343 nm. The observed blue-shift was more pronounced for **(DAT-Toct)$_2$**, which has an absorbance maximum located at 329 nm. The solution absorbance results for the barbiturate (B) derivatives are generally red-shifted by more than 100 nm compared to the DAT compounds, with maximum absorbance (λ_{max}) values of 486, 453, and 437 nm for **(B-T)$_2$**, **(B-TMe)$_2$**, and **(B-Toct)$_2$**, respectively

Table 1 Summary of experimental and theoretical (DFT) optoelectronic properties of DAT, B, PH, and PMe compounds

Target molecule	S–C–C–S dihedral angle (°)	HOMO (eV)	LUMO (eV)	$E_{g\text{-}DFT}$[b] (eV)	λ_{onset} (nm)	$E_{g\text{-}opt}$[c] (eV)	$E_{relative}$[b] (kcal mol^{-1})
(DAT-T)$_2$	15	−5.67	−2.30	3.37	421	2.95	0
(DAT-T)$_2$[a]	0	−5.63	−2.31	3.32	———	———	+0.08
(DAT-TMe)$_2$	51	−5.76	−2.01	3.75	412	3.00	0
(DAT-TMe)$_2$[a]	0	−5.45	−2.17	3.28	———	———	+1.23
(DAT-Toct)$_2$	68	−5.94	−1.85	4.09	389	3.19	0
(DAT-Toct)$_2$[a]	0	−5.41	−2.15	3.26	———	———	+3.88
(B-T)$_2$	0	−6.56	−3.90	2.66	556	2.23	———
(B-TMe)$_2$	38	−6.50	−3.71	2.79	553	2.24	———
(B-Toct)$_2$	———	———	———	———	515	2.41	———
(PH-T)$_2$	18	−5.93	−2.82	3.11	469	2.64	———
(PMe-T)$_2$	21	−5.76	−2.57	3.19	465	2.67	———
(PH-TMe)$_2$	57	−6.02	−2.61	3.41	463	2.68	———
(PMe-TMe)$_2$	62	−5.90	−2.34	3.56	461	2.69	———
(PH-Toct)$_2$	72	−6.13	−2.52	3.61	448	2.77	———
(PMe-Toct)$_2$	72	−5.97	−2.26	3.71	———	———	———

Note: All theoretical (DFT) data are based on geometry optimizations at the B3LYP/6-31+G(d) level of theory.[57]
[a]Data derived from molecules constrained to planarity.
[b]Determined from DFT calculations.
[c]Determined from experimental UV-vis data in DMSO.

(Figure 4a). This observation is attributed to the strong electron-withdrawing nature of the barbiturate unit compared to DAT, which stabilizes the LUMO of the barbiturate derivatives and narrows the HOMO–LUMO gap, an observation confirmed by theoretical calculations (Table 1). Like the DAT family, a hypsochromic shift was observed for the B family upon incorporation of increasingly larger R groups (R = H, Me, *n*-octyl). This observation is reflected qualitatively by the color change of each compound in solution, wherein increasing steric demands caused by the R group substitution results in more colorless solutions for the DAT family (Figure S1, Supporting Information) and B family (Figure S2, Supporting Information), respectively.[58] For the PH derivatives, a single absorption band was observed for all compounds in the UV region, similar to the DAT derivatives. The non-alkylated **(PH-T)$_2$** showed the most red-shifted absorbance (λ_{max} = 409 nm), whereas the HB-incapable comparator **(PMe-T)$_2$** exhibits a similar optical response with an absorbance maximum at 404 nm (Figure 4b). An evident blue-shift was observed upon introduction of alkyl groups onto the bithiophene unit (R = Me), resulting in λ_{max} values of 369 nm for **(PH-TMe)$_2$** and 361 nm for the HB-incapable comparator, **(PMe-TMe)$_2$**, respectively (Figure 4b). Similar to the trends observed for the DAT and B derivatives, the blue-shift is enhanced when *n*-octyl chains are installed on the PH bithiophene linker, resulting in a λ_{max} value at 358 nm for **(PH-Toct)$_2$** (Figure 4b). The *n*-octyl-substituted HB-incapable comparator, **(PMe-Toct)$_2$**, is a liquid and the UV-vis absorbance was not measured due to difficulties in measuring the mass of the sample. For all studied derivatives, no aggregation was observed for the DAT, B, and PH compounds within the selected concentration ranges (2.5–30 μM) as evidenced by the Beer–Lambert plots obtained for DAT derivatives (Figure S3, Supporting Information), barbiturate derivatives (Figure S4, Supporting Information), and PH derivatives (Figure S5–S6, Supporting Information).

The trends observed in the absorption maxima for DAT, B, and PH derivatives, and the associated color changes for DAT and B compounds in solution (Figure S1–S2, Supporting Information), can be attributed to the increasing steric demands introduced by the increasing size of the bithiophene R groups (R = H, Me, *n*-octyl).[59] Installation of the alkyl chains causes twisting about the sigma bond connecting the thiophene units of the 2,2′bithiophene linker, resulting in an increase in the S–C–C–S dihedral angle as the size of the R group increases. This conformational change acts to relieve torsional strain, but in turn results in a reduction of the π-conjugation. To verify this analysis, theoretical calculations (DFT) were performed on all compounds at the B3LYP/6-31+G(d) level of theory.[57] As suspected, the planarity of each molecule decreases upon increasing R group size, an observation which is reflected by the increasing dihedral angle (S–C–C–S) between adjacent thiophenes, equal to 15°, 51°, and 68° for **(DAT-T)$_2$**, **(DAT-TMe)$_2$**, and **(DAT-Toct)$_2$**, respectively (Table 1, Figure S7). A

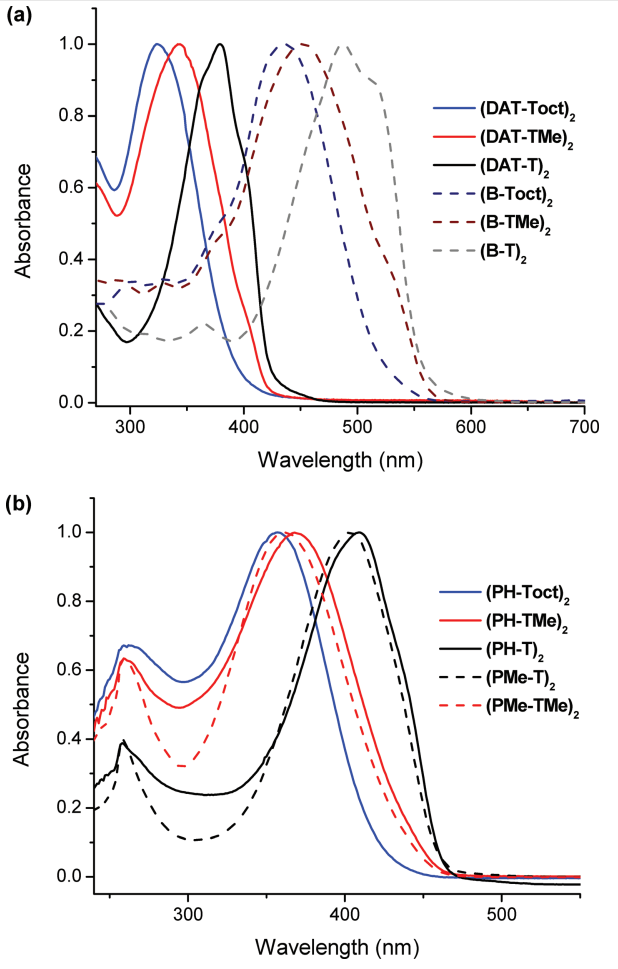

Figure 4 Normalized absorption spectra (20 mM, DMSO) of (a) diaminotriazine (DAT) and barbiturate (B) compounds (R = H, Me, and *n*-octyl), and (b) phthalhydrazide (PH) and phthalic methyl esters (PMe).

similar trend was observed for the barbiturate family, wherein the DFT-optimized geometries showed dihedral angles of 0° and 38° for **(B-T)$_2$** and **(B-TMe)$_2$**, respectively (Table 1, Figure S8). Optimization attempts on **(B-Toct)$_2$** were unfortunately not successful due to repeated convergence failures associated with the long *n*-octyl chains. DFT optimizations of the PH derivatives showed a similar trend, wherein the S–C–C–S torsion increases from 18°, 57°, and 72° for **(PH-T)$_2$**, **(PH-TMe)$_2$**, and **(PH-Toct)$_2$**, respectively (Table 1, Figure S9). Similar results were obtained for the HB-incapable comparators, with dihedral values of 21°, 62°, and 72° were observed for **(PMe-T)$_2$**, **(PMe-TMe)$_2$**, and **(PMe-Toct)$_2$**, respectively (Table 1, Figure S9). In general, the data obtained from absorption studies agreed with the trends observed from the theoretical geometries.

To gain more insight into the effect of molecular twisting on the electronic properties, additional DFT optimizations were performed with DAT molecules which were constrained to planarity (S–C–C–S dihedral angle = 0°) (Table 1, Figure S10). For the planarized structures (Figure S10), the HOMO energy level increases while the LUMO orbital energy decreases (Table 1). The net result is a narrowing of the frontier molecular orbital energy gap, which can be attributed to the increase in π-conjugation in the more planar structures. These changes are most pronounced with the *n*-octyl derivative **(DAT-Toct)$_2$**, consistent with the large difference in dihedral angle between the unconstrained geometry (S–C–C–S dihedral = 68°) and the fully constrained geometry (S–C–C–S dihedral = 0°). The associated energetic penalties are an informative result, with the planarity constraint increasing the gas-phase energy, ranging from 0.08 to 3.88 kcal mol^{-1} for **(DAT-T)$_2$** and **(DAT-Toct)$_2$**, respectively (Table 1).

Vacuum thermal evaporation was selected as the deposition technique for solid-state studies because this method can provide greater control over film thickness and is better suited for microscopic and photophysical investigations. Prior to processing, the thermal stability of each target molecule was investigated using TGA. The DAT and B compounds showed suitably high thermal stabilities, with 5% weight loss values ranging between 329 and 354 °C for the DAT derivatives and 307 and 368 °C for the B derivatives, respectively, indicating that these compounds should likely survive vacuum thermal evaporation with their structures intact (Figure S19, Supporting Information). The TGA data for the PH compounds showed thermal stabilities with a 5% mass loss ranging between 225 and 414 °C, indicating thermal instability of some of the PH derivatives (Figure S19, Supporting Information). **(PMe-Toct)$_2$** is a liquid and therefore was not suitable for TGA analysis. In all cases, the TGA curves showed a stepwise decomposition process. Attempts to analyze the curves and relate % mass loss to a removal of any specific unit from the molecule were inconclusive. For **(PH-T)$_2$**, ^{1}H NMR studies were conducted, and ^{1}H NMR spectra of the as-synthesized substrate were compared with samples heated to 180 °C (Figure S11, Supporting Information). While the characteristic resonances persisted, it was observed that the integration ratio of the signals associated with the aromatic phenyl protons did not match the fresh sample, possibly indicating thermal decomposition associated with the phenyl ring during the heating process (Figure S11, Supporting Information).

Based on the TGA data, it was determined that the DAT and B compounds were most amenable to the vacuum thermal evaporation process. The DAT and barbiturate films were subsequently deposited on clean silicon substrates in a custom high vacuum chamber (base pressure ~1 × 10^{-6} Torr) with varying deposition rates and thicknesses. The post-deposition structural integrity was evaluated from ^{1}H NMR analysis of a suitably thick film (re-dissolved from the film into DMSO-d_6), and the ^{1}H NMR spectra were

compared to the ^{1}H NMR spectra of the as-synthesized materials. Structural integrity of all DAT and B materials were confirmed from the post-deposition NMR studies, with the exception of the non-alkylated barbiturate compound, **(B-T)$_2$**, an important result to consider if it is assumed that the structural integrity, upon deposition, of such molecules is warranted (Figure S15, Supporting Information). Further attempts to optimize the vacuum thermal deposition conditions for **(B-T)$_2$** were not successful.

With the deposition conditions optimized for the remaining oligomers, solid-state optical properties were investigated using 70 ± 5 thick films (Figure 5). The solid-state absorbance for all studied compounds was red-shifted significantly with respect to the corresponding solution absorbance (Table 2). Thin-film absorbance maxima (λ_{max}) of 399, 376, and 357 nm were observed for **(DAT-T)$_2$**, **(DAT-TMe)$_2$**, and **(DAT-Toct)$_2$**, respectively (Figure 5a). For the barbiturate derivatives, absorbance maxima of 535 and 480 nm were observed for **(B-TMe)$_2$** and **(B-Toct)$_2$**, respectively (Figure 5b). The observed red-shifts in maximum absorbance are largely attributed to improved molecular overlap, enhanced planarity, and better packing of the molecules in the solid state.[24,25,60–62] Both *n*-octyl derivatives, **(DAT-Toct)$_2$** and **(B-Toct)$_2$**, showed featureless absorption profiles in the solid-state spectra. For the other derivatives, a slight shouldering was observed in the thin-film optical response, including more pronounced vibrational absorbance characteristics associated with **(B-TMe)$_2$**. The more complex absorbance profile for **(B-TMe)$_2$** could possibly indicate a higher degree of molecular ordering, enhanced planarity and aggregation, which could result in the formation of excimers.[63,64] Upon closer analysis of solid-state absorbance profiles, a general red-shift in absorbance maxima is observed for the neat films compared to solution, a trend which was not observed in all cases in our previous work on monotopic derivatives (Table 2).[25] A 21 nm red-shift was observed for **(DAT-T)$_2$** in the solid state compared to solution; this difference increases to 33 nm for **(DAT-TMe)$_2$**. These trends can be attributed to the significantly improved planarity of **(DAT-TMe)$_2$** considering the transition from solution to the solid state. In agreement with the theoretical (DFT) simulations, it can be concluded that **(DAT-T)$_2$** enjoys a nearly planar geometry in solution, and the transition from solution to solid state results in only minimal changes in the bithiophene dihedral angle. The change in absorbance maximum for **(DAT-Toct)$_2$** is 28 nm going from solution to the solid state. This seemingly minimal change might be attributed to less effective stacking of the *n*-octyl-substituted molecule compared to the methyl-substituted **(DAT-TMe)$_2$**. Similar but significantly pronounced differences were observed between the solution and solid-state absorbance of the barbiturate derivatives **(B-TMe)$_2$** ($\Delta\lambda_{max}$ = 82 nm red-shift, solid state) and **(B-Toct)$_2$** ($\Delta\lambda_{max}$ = 43 nm red-shift, solid state). The solid-state absorbance of **(B-T)$_2$** was not collected due to

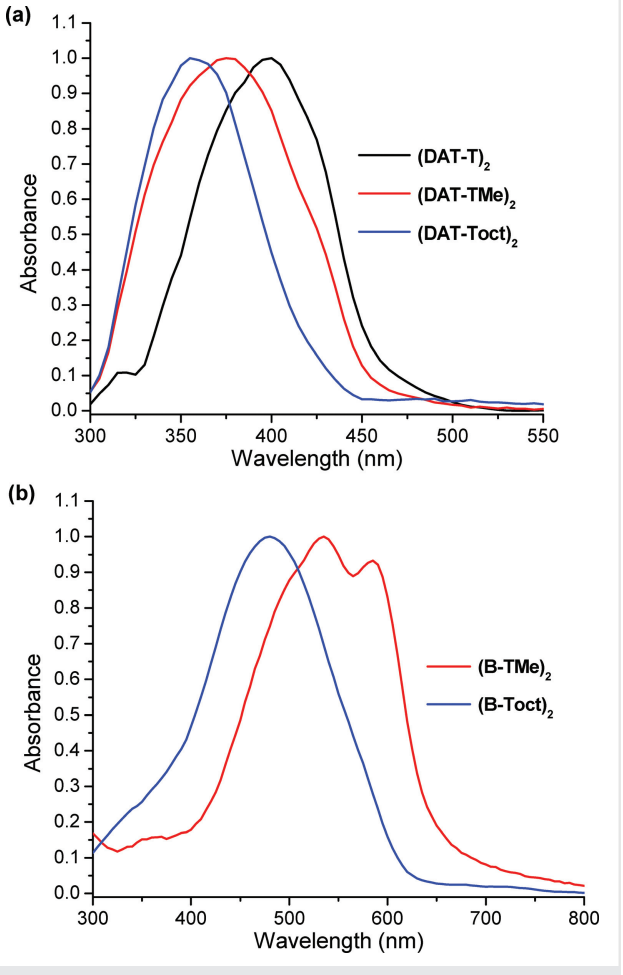

Figure 5 Normalized thin-film absorbance spectra for (a) **(DAT-T)$_2$**, **(DAT-TMe)$_2$**, and **(DAT-Toct)$_2$**; (b) **(B-TMe)$_2$** and **(B-Toct)$_2$**.

Table 2 Solution (DMSO) versus solid-state (neat-film) optical properties

	UV-vis (DMSO solution)[a]			UV-vis (neat film)[b]		
	λ_{max}	λ_{onset}	$E_{g\text{-}opt}$	λ_{max}	λ_{onset}	$E_{g\text{-}opt}$
Compound	(nm)	(nm)	(eV)	(nm)	(nm)	(eV)
(DAT-T)$_2$	378	421	2.95	399	472	2.63
(DAT-TMe)$_2$	343	412	3.00	376	456	2.72
(DAT-Toct)$_2$	329	389	3.19	357	441	2.82
(B-T)$_2$	486	556	2.23	———	———	———
(B-TMe)$_2$	453	553	2.24	535	660	1.88
(B-Toct)$_2$	437	515	2.41	480	622	2.00

[a]Determination made based on UV-vis data in DMSO.
[b]Determined from thin-film absorption data.

decomposition issues associated with the deposition process.

Each of the DAT derivatives, **(DAT-T)$_2$**, **(DAT-TMe)$_2$**, and **(DAT-Toct)$_2$**, was successfully deposited onto a Au(111) substrate under UHV conditions, and the supramolecular assemblies were investigated via STM. The **(DAT-T)$_2$** monolayer displayed a highly ordered superstructure on the Au(111) surface, with both short-range and long-range periodicities (Figure 6). Looking closely at the images, formation of an interdigitated hexameric arrangement composed of six **(DAT-T)$_2$** molecules was observed across the surface with a periodicity of 2.75 nm between the central points of two adjacent rosettes (Figure 6a). Formation of these molecular arrangements is guided by 12 intermolecular HB interactions between the amine H-atoms and the triazine N-atoms of adjacent **(DAT-T)$_2$** molecules. Each molecule participates in four HB interactions from the same end of the molecule while the other HB-functionalized end does not show clear signs of HB interactions with adjacent molecules. This is likely attributed to the consequence of maximizing the packing density of molecules to minimize the system energy. Even though **(DAT-T)$_2$** is an achiral molecule, a chiral recognition was observed from the STM images upon assembly, giving rise to both clockwise and counterclockwise enantiomeric rosettes as represented by the blue and green arrows highlighted in the STM image (Figure 6b). Overall, the results obtained here are consistent with the assembly motifs observed for monotopic systems on surfaces and at the solid–liquid interface.[36,40,41,65] Thermal annealing of the **(DAT-T)$_2$** monolayer (500 K) resulted in reorganization of the molecules, giving rise to a different assembly pattern (Figure 7). The introduction of thermal energy into the system disrupts the directing intermolecular forces and results in a two-dimensional, closely packed linear arrangement composed of a series of one-dimensional (1D) parallel chains (Figure 7). This linear-type arrangement is consistent with the results obtained for a ditopic DAT molecule reported by Fasel and co-workers.[66] Unlike the hexameric rosette formation which results from four HB-interactions per molecule, in the linear arrangement each **(DAT-T)$_2$** molecule participates in eight non-covalent (HB) interactions per molecule, leading to a more thermodynamically stable assembly. It seems that the hexameric assembly is a kinetically trapped arrangement, and that the introduction of thermal energy causes molecular reorganization to yield the more thermodynamically favored linear superstructure. Long-range ordering was observed in the linear arrangement as well (length = 1.66 ± 0.1 nm and width = 0.67 ± 0.2 nm). The observed geometry was consistent with the results obtained from DFT calculations, wherein nearly identical molecular dimensions were observed for a monomeric unit (length = 1.64 nm and width = 0.69 nm, B3LYP/6-31+G(d) level of theory).[57]

For **(DAT-TMe)$_2$**, the closely packed linear arrangement was also observed by STM, both before and after thermal annealing at 500 K (Figure 8). The molecular dimensions

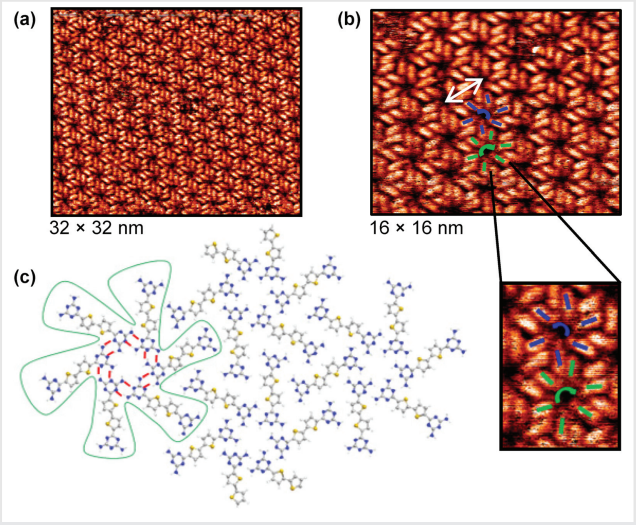

Figure 6 Constant current STM images (a, b) and structure model (c) of **(DAT-T)$_2$** overlayer on Au(111) as deposited at room temperature. Regions of molecular ordering composed of interdigitated DAT hexamers are observed across the surface. Clockwise and anticlockwise clusters are represented by blue and green arrows. White double arrow indicates the distance between centers of adjacent rosettes (2.75 nm). Red lines in the structure model indicate the proposed H-bonds. (tunneling conditions: V_b = 0.7 V, I_t = 0.05 nA).

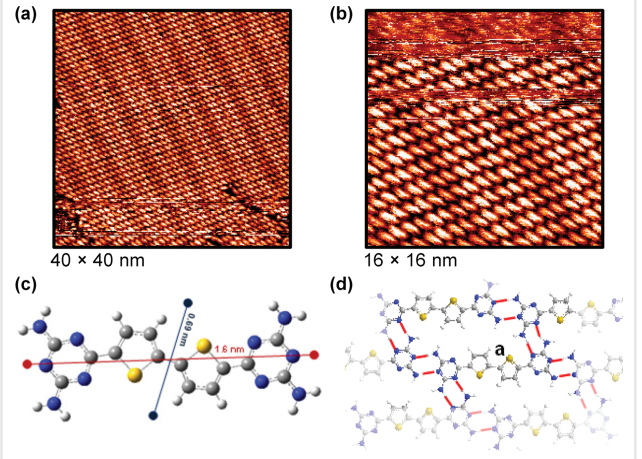

Figure 7 (a and b) STM images of **(DAT-T)$_2$** showing the ordered structure formed at monolayer coverage after annealing at 500 K. Each chain is formed through the head-to-tail H-bond association of adsorbates, with the adsorbate dimensions: length of 1.66 ± 0.11 nm, and width of 0.67 ± 0.02 nm, consistent with results obtained from DFT calculations at the B3LYP/6-31+G(d) level.[57] (c) In the structural model (d), red lines indicate the proposed H-bonds and the formation of eight H-bonds is shown in the molecule designated by letter "**a**" (tunneling conditions: V_b = 0.7 V, I_t = 0.05 nA).

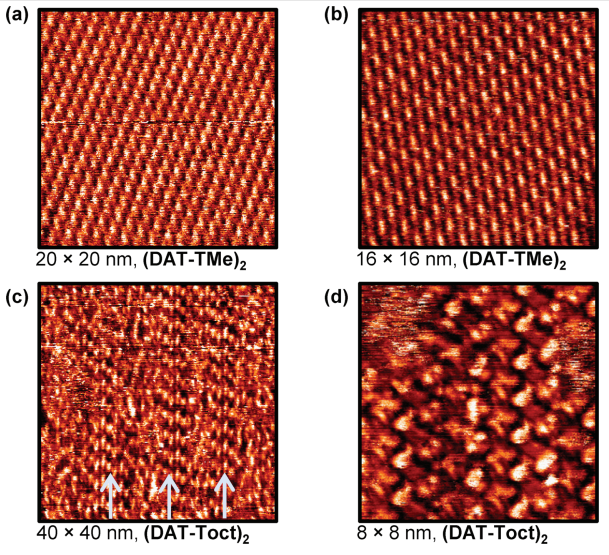

Figure 8 (a, b) Constant current STM images of **(DAT-TMe)$_2$** overlayer on Au(111) after annealing at 500 K for 10 min (tunneling conditions: $V_b = 1.5$V, $I_t = 0.05$ nA). (c, d) Constant current STM images of **(DAT-Toct)$_2$** overlayer on Au(111) after annealing at 500 K for 10 min. Blue arrows indicate linear chain arrangement (tunneling conditions: $V_b = 1.5$V, $I_t = 0.05$ nA).

were observed to be slightly larger for **(DAT-TMe)$_2$** (length = 1.73 nm and width = 0.77 nm) compared to **(DAT-T)$_2$**, which can be rationalized through the expected increase in size of the structure due to the inclusion of methyl substituents on the bithiophene backbone. The methyl substituents also likely prevented the formation of the interdigitated rosette assemblies observed for **(DAT-T)$_2$**. For **(DAT-Toct)$_2$**, an irregular linear arrangement was observed in the STM images, a superstructure possibly influenced by the sterically congested *n*-octyl substituents (Figure 8). The supramolecular ordering prevails with a head-to-tail arrangement of the **(DAT-Toct)$_2$** molecules resulting in a 1D assembly (Figure 8c, gray arrows). However, the long-range HB interactions observed for both **(DAT-T)$_2$** (post-annealing) and **(DAT-TMe)$_2$** (pre- and post-annealing) were absent in the case of the *n*-octyl-substituted derivative, presumably disrupted by the bulky *n*-octyl chains.

For the barbiturate derivatives, similar attempts were made to investigate the mono-layer structure on Au(111) by STM. While the non-alkylated derivate, **(B-T)$_2$**, was unable to survive the vacuum thermal deposition conditions (Figure S15, Supporting Information), the methyl-substituted barbiturate derivative **(B-TMe)$_2$** showed several co-existent assemblies (Figure S18, Supporting Information). The result contrasts with the more familiar solution-phase assembly of barbiturate derivatives into six-membered rosettes, which even persists at the solid–liquid interface as reported by Yagai and coworkers.[23,46,47] The difference presumably reflects the different thermodynamic and kinetic aspects associated with deposition on Au(111) (versus highly oriented pyrolytic graphite HOPG) and by UHV. The complexity of the STM results for **(B-TMe)$_2$** and time/cost intensity of these experiments dissuaded us from systematically studying or optimizing the sample preparation or from attempting similar studies with the more difficultly processed **(B-Toct)$_2$**. Attempting to derive relationships between the observed superstructure for **(B-TMe)$_2$** and molecular structure in this case is difficult and speaks directly to some of the challenges in this research area.

Conclusions

Three families of novel, but simple, π-conjugated 2,2′-bithiophenes capped on both termini with HB-capable units, diaminotriazine (DAT), barbiturate (B), and phthalhydrazide (PH), were designed and synthesized. These designs were elaborated with different R groups on the bithiophene unit (R = H, Me, *n*-octyl) to study the effects of solubilizing group substitution on the photophysical properties and solid-state organization of these species. Additionally, three HB-incapable phthalic ester comparator molecules were studied, isolated as advanced intermediates during the synthesis of the final, HB-capable, PH targets. The effects of solubilizing group substitution on the optoelectronic properties were first studied computationally by DFT (gas-phase, B3LYP/6-31+G(d) level of theory)[57] and in solution by UV-vis spectroscopy. All compounds showed a blue-shift in solution absorbance with increasing size of the alkyl substituents on the bithiophene linker, a consequence of relieving torsional strain which in turn decreases the extent of π-conjugation in the molecules.[59] Thermal stabilities of the targets were assessed with TGA, where modest to good thermal stabilities were observed. Structure–arrangement relationships for selected substrates were established by STM. The non-alkylated structure, **(DAT-T)$_2$**, showed an ordered arrangement of hexameric rosettes on the Au(111) surface. Upon thermal annealing (500 K), an ordered linear arrangement with a higher number of HB interactions per molecule was achieved as the more thermodynamically favored superstructure. A similar linear motif was observed for **(DAT-TMe)$_2$** by STM before and after thermal annealing. The STM results indicate that HB interactions are preserved in all cases, but the observed arrangements on the substrate are strongly dictated by a balance of stabilizing intermolecular non-covalent interactions, molecule–substrate interactions, and de-stabilizing sterically repulsive interactions. The influence of the solubilizing group was the most pronounced in the case of the *n*-octyl-substituted derivative, **(DAT-Toct)$_2$**, which resulted in an irregular linear arrangement observed by STM

in the monolayer. In the case of the barbiturate (B) derivatives, **(B-TMe)$_2$** showed multiple assembly structures co-existing together on the same substrate after vacuum thermal evaporation. The molecular–supramolecular relationships developed in this study will be useful in the design of self-assembling organic materials for future electronic and optoelectronic applications.

Experimental Section

General Methods

Reagents and solvents were purchased from commercial sources and used without further purification unless otherwise specified. THF and DMF were degassed in 20 L drums and passed through two sequential purification columns under a positive argon atmosphere. TLC was performed on SiO_2-60 F_{254} aluminum plates with visualization by UV light or staining. Flash column chromatography was performed using silica gel technical grade, pore size 60 Å, 230–400 mesh particle size, 40–63 µm particle size from Sigma-Aldrich. ^{1}H (^{13}C) NMR spectra were recorded on Mercury 300 or INOVA 500 spectrometer. Chemical shifts (δ) are given in parts per million (ppm) relative to TMS and referenced to residual protonated solvent purchased from Cambridge Isotope Laboratories, Inc. ($CDCl_3$: δH 7.26 ppm, δC 77.16 ppm; DMSO-d_6: δH 2.50 ppm, δC 39.52 ppm). Abbreviations used are s (singlet), d (doublet), t (triplet), q (quartet), quin (quintet), hp (heptet), b (broad), and m (multiplet). Electrospray ionization (ESI) HRMS spectra were recorded on an Agilent 6210 TOF spectrometer with MassHunter software. Intermediate **1** was synthesized according to the literature precedent.[52] Intermediate **8** was synthesized according to the literature precedent.[67]

Computational Analysis

The final ground-state geometries and orbital energies of the molecules were obtained from DFT calculations at the B3LYP/6-31+G(d) level as implemented in Gaussian 09,[57] accessed through the University of Florida High Performance Computing Center. The models in Figures 6c and 7d were generated using the MacroModel program (Maestro Release 2016-3) and the Amber* force field.

Thermogravimetric Analysis

TGA measurements were performed using ~2 mg of sample on TA Instruments Q5000-0121 (platinum pan, room temperature to 600 °C, ramp rate = 20 °C min^{-1} under nitrogen atmosphere) and analyzed using Universal Analysis 2000 4.4A software. The compounds were heated and held first at 60 °C for 30 min to remove any remaining solvent before full TGA analysis was performed.

Thin-Film Preparation

To study the self-assembly of the DAT and B simple ditopic compounds, thin films were thermally evaporated onto various substrates including clean silicon wafers and glass substrates in a custom high vacuum chamber (base pressure ~1×10^{-6} Torr). Thicknesses of the deposited films were monitored using a calibrated quartz crystal monitor, and a deposition rate in the range of 0.2 to 0.5 Å/s was achieved by adjusting the heating power applied on the source boats. Film thicknesses were calibrated using a Dektak profilometer, resulting in an accuracy typically within 10%.

Solution and Solid-State Absorption

Solution absorption spectra of the compounds were measured on a Perkin-Elmer Lambda 25 dual beam absorption spectrometer and a Cary 100 Bio spectrophotometer using 1 cm quartz cells. The absorption intensity at λ_{max} was then plotted against the concentration in all cases to confirm, by linearity, whether the compounds followed the Beer–Lambert law. Molar extinction coefficients (ε) were determined from the linear plot for each compound (where $A = \varepsilon bc$).

To measure solid-state (thin film) absorption, monochromatic light was shone incident on to the film and chopped by a mechanical chopper and absorbance was measured using a Newport 818 UV detector connected to a pre-amp and lock-in amplifier.

Scanning Tunneling Microscopy

The Au(111) substrate was prepared by annealing Au films on mica with a hydrogen–oxygen flame ex-situ. The sample was immediately introduced into the UHV chamber through a load-lock, and then annealed at 500 K for 20 min in order to remove contaminants on the surface. Molecules were evaporated in UHV from a Ta evaporation source. A type-K thermocouple was spot-welded to the outer surface of the source in order to monitor the evaporation temperature. The Au(111) substrate was kept at room temperature during evaporation.

Molecular assemblies were imaged, following deposition, using a variable temperature STM equipped with cooling–heating facilities providing access to the temperature range 25–750 K (Omicron Nanotechnology)

with ±1 K precision. The microscope was mounted in an ion pumped UHV chamber with a base pressure of $<2 \times 10^{-10}$ Torr. The tip was made by electrochemically etching tungsten wire with a diameter of 0.25 mm in 3 M NaOH solution. STM images were collected under conditions of constant current.

Procedures

[2,2'-Bithiophene]-5,5'-dicarbonitrile (2): To a 100 mL three-necked round-bottom flask was added **1** (0.20 g, 0.90 mmol), ammonia (3.7 mL, 54 mmol, c.a. 28% aqueous solution), and anhydrous THF (5 mL). With stirring, iodine (0.68 g, 2.7 mmol) dissolved in anhydrous THF (5 mL) was added slowly via an addition funnel. The reaction mixture was stirred for 12 hours at room temperature, and then quenched with aqueous $Na_2S_2O_3$ solution (ca. 5%, 25 mL). The mixture was extracted with methylene chloride (DCM), and the organic layers were combined and dried over anhydrous Na_2SO_4. After filtration and evaporation under reduced pressure, the residue was purified by column chromatography on silica gel (ethyl acetate/hexanes = 3/7) to give a yellow solid (0.097 g, 0.45 mmol, 50%).[68] ^{1}H NMR (300 MHz, DMSO-d_6) $\delta = 8.03$ (d, $J = 3.5$ Hz, 2 H), 7.72 (d, $J = 2.9$ Hz, 2 H).

4,4,5,5-Tetramethyl-2-(3-methylthiophen-2-yl)-1,3,2-dioxaborolane (3): A 3-necked round-bottom flask containing 2-bromo-3-methylthiophene (2.0 g, 11 mmol) was equipped with a stir bar and two septa. The flask was flushed with argon three times. Anhydrous THF (15 mL) was added to the flask. The mixture was cooled to −78 °C. *n*-butyllithium (6.9 mL, 17 mmol) was added dropwise to the mixture. The mixture was maintained at −78 °C and allowed to stir for 2 hours. 2-Isopropoxy-4,4,5,5-tetramethyl-1,3,2-dioxaborolane (2.5 g, 14 mmol) was added to the mixture. The mixture was allowed to warm and stirred for 14 hours. The solvent was removed and the resulting concentrate was purified by column chromatography on silica gel (DMC/hexanes = 1/2) to give a white solid (1.9 g, 8.8 mmol, 80%). The carbon directly attached to boron was undetectable, presumably due to quadrupolar relaxation. The NMR data matched the literature values.[56] ^{1}H NMR ($CDCl_3$, 300 MHz): $\delta = 7.48$ (d, $J = 5.0$ Hz, 1 H), 6.97 (d, $J = 4.7$ Hz, 1 H), 2.48 (s, 3 H), 1.33 (s, 12 H). ^{13}C NMR ($CDCl_3$, 125 MHz): $\delta = 148.97$, 131.36, 83.54, 24.84, 16.05.

3,3'-Dimethyl-2,2'-bithiophene (4): Under argon, anhydrous toluene (10 mL) and degassed water (1.3 mL) were added to a two-necked round-bottom flask containing **3** (0.25 g, 1.2 mmol), 2-bromo-3-methylthiophene (0.25 g, 1.4 mmol), sodium carbonate (0.35 g, 3.4 mmol), and tetrakis(triphenylphosphine)palladium (0) (0.13 g, 0.11 mmol). The reaction mixture was heated at 100 °C for 20 hours. After cooling to room temperature, the mixture was poured into water and extracted with DCM. The organic layer was collected, washed with water, and dried over Na_2SO_4. The solvent was evaporated under reduced pressure and the crude product was purified by gradient column chromatography on silica gel (CH_2Cl_2/hexanes = 0/10 to 1/9) to give the pure product as a colorless oil (0.17g, 0.87 mmol, 78%). The NMR data matched the literature values.[69] ^{1}H NMR ($CDCl_3$, 500 MHz): $\delta = 7.32$ (d, $J = 5.2$ Hz, 2 H), 6.98 (d, $J = 5.2$ Hz, 2 H), 2.24 (s, 6 H). ^{13}C NMR ($CDCl_3$, 125 MHz): $\delta = 136.62$, 130.14, 129.52, 125.10, 14.81.

3,3'-Dimethyl-[2,2'-bithiophene]-5,5'-dicarbaldehyde (5): To cold, dry DMF (3 mL) at 0 °C, $POCl_3$ (1.5 mL, 10 mmol) was added dropwise and the solution was stirred for 1 h. Then **4** (0.10 g, 0.52 mmol), dissolved in anhydrous DMF (1 mL), was added to the mixture using a syringe and the reaction was heated to reflux at 100 °C for 15 hours under argon. After cooling to room temperature, the reaction mixture was poured into ice water (25 mL), neutralized with saturated NaOH solution, and then extracted with dichloromethane (DCM). The combined organic layer was washed with H_2O, dried over Na_2SO_4, and evaporated under reduced pressure. The crude product was purified by column chromatography on silica gel (CH_2Cl_2/hexanes = 3/2) to give a yellow solid (0.052 g, 0.21 mmol, 40%). ^{1}H NMR ($CDCl_3$, 300 MHz): $\delta = 9.89$ (s, 2 H), 7.63 (s, 2 H), 2.30 (s, 6 H). ^{13}C NMR ($CDCl_3$, 125 MHz): $\delta = 182.84$, 143.06, 138.94, 138.81, 138.34, 15.32. HRMS (ESI): m/z $[M + H]^+$ calcd for $C_{12}H_{10}O_2S_2$: 251.0198; found: 251.0198.

3,3'-Dimethyl-[2,2'-bithiophene]-5,5'-dicarbonitrile (6): To a 100 mL three-necked round-bottom flask was added **5** (0.20 g, 0.90 mmol), ammonia (3.7 mL, 54 mmol, c.a. 28% aqueous solution), and anhydrous THF (5 mL). With stirring, iodine (0.68 g, 2.7 mmol), dissolved in anhydrous THF (5 mL), was added slowly via an addition funnel. The reaction mixture was stirred for 12 hours at room temperature, and then quenched with aqueous $Na_2S_2O_3$ solution (ca. 5%, 25 mL). The mixture was extracted with DCM, and the organic layers were combined and dried over anhydrous Na_2SO_4. After filtration and evaporation under reduced pressure, the residue was purified by column chromatography on silica gel (ethyl acetate/hexanes = 3/7) to give a yellow solid (0.097 g, 0.40 mmol, 50%). ^{1}H NMR ($CDCl_3$, 300 MHz): $\delta = 7.48$ (s, 2 H), 2.21 (s, 6 H). ^{13}C NMR ($CDCl_3$, 125 MHz): $\delta = 139.99$, 138.76, 134.14, 113.66, 110.56, 14.85. HRMS (ESI): m/z $[M + H]^+$ calcd for $C_{12}H_8N_2S_2$: 245.0202; found: 245.0193.

2-Bromo-3-octylthiophene (7): A 3-necked round-bottom flask containing 3-*n*-octylthiophene (0.39 g, 2.0 mmol) and *N*-bromosuccinimide (0.36 g, 2.0 mmol) was equipped with a stir bar and two septa. The flask was flushed with argon three times. Chloroform (15 mL) was added to the flask. The mixture was cooled to 0 °C.

Glacial acetic acid (1 mL) was added. The mixture was warmed to room temperature and stirred overnight. The mixture was neutralized in a separatory funnel with saturated sodium bicarbonate (10 mL). The organic components were extracted into DCM and were dried over anhydrous sodium sulfate. The solvent was removed and the resulting concentrate was purified by silica gel column chromatography (hexanes) to give a colorless oil (0.52 g, 1.9 mmol, 95%). The NMR data matched the literature values.[67] ^{1}H NMR ($CDCl_3$, 500 MHz): $\delta = 7.18$ (d, $J = 5.6$ Hz, 1 H), 6.79 (d, $J = 5.6$ Hz, 1 H), 2.56 (t, $J = 7.7$ Hz, 2 H), 1.60–1.54 (m, 2 H), 1.36–1.22 (m, 10 H), 0.88 (t, $J = 6.9$ Hz, 3 H). ^{13}C NMR ($CDCl_3$, 150 MHz): $\delta = 142.13$, 128.38, 125.26, 108.93, 32.03, 29.88, 29.55, 29.53, 29.39, 29.38, 22.82, 14.26.

3,3'-Dioctyl-[2,2'-bithiophene]-5,5'-dicarbaldehyde (9): Anhydrous and deoxygenated toluene (6 mL) was added into a mixture of $Pd(OAc)_2$ (0.020 g, 0.085 mmol) and diisopropylethylamine (0.22 g, 1.7 mmol). Into the solution was introduced 5-bromo-4-octylthiophene-2-carbaldehyde (0.50 g, 1.7 mmol) and tetrabutylammonium bromide (0.30 g, 0.85 mmol) and the resulting solution was degassed and then heated to reflux for 20 h. The reaction mixture was cooled, poured into water, and extracted with DCM. The combined organic layers were washed with H_2O, dried over Na_2SO_4, and evaporated under reduced pressure. The crude product was purified by column chromatography using silica (CH_2Cl_2/hexanes = 3/2) to give a yellow solid (0.15 g, 0.34 mmol, 41%). The NMR data matched the literature values.[55] ^{1}H NMR ($CDCl_3$, 300 MHz): $\delta = 9.89$ (s, 2 H), 7.66 (s, 2 H), 2.56 (t, $J = 8.4$ Hz, 4 H), 1.61–1.53 (m, 4 H), 1.33–1.21 (m, 20 H), 0.88 (t, $J = 6.6$ Hz, 6 H). ^{13}C NMR ($CDCl_3$, 75 MHz): $\delta = 182.90$, 144.61, 143.58, 137.63, 137.57, 31.69, 30.66, 29.43, 29.41, 29.28, 29.02, 22.77, 14.23.

3,3'-Dioctyl-[2,2'-bithiophene]-5,5'-dicarbonitrile (10): To a 100 mL three-necked round-bottom flask was added **9** (0.20 g, 0.90 mmol), ammonia (3.7 mL, 54 mmol, c.a. 28% aqueous solution), and anhydrous THF (5 mL). With stirring, iodine (0.68 g, 2.7 mmol), dissolved in anhydrous THF (5 mL), was added slowly via an addition funnel. The reaction mixture was stirred for 12 hours at room temperature, and then quenched with aqueous $Na_2S_2O_3$ solution (ca. 5%, 25 mL). The mixture was extracted with DCM, and the organic layers were combined and dried over anhydrous Na_2SO_4. After filtration and evaporation under reduced pressure, the residue was purified by column chromatography on silica gel (ethyl acetate/hexanes = 3/7) to give a yellow solid (0.097 g, 0.22 mmol, 50%). ^{1}H NMR ($CDCl_3$, 300 MHz): $\delta = 7.50$ (s, 2 H), 2.48 (t, $J = 8.0$, 4 H), 1.20–1.25 (m, 20 H), 0.88 (t, $J = 7.2$ Hz, 6 H). ^{13}C NMR ($CDCl_3$, 125 MHz): $\delta = 144.49$, 138.73, 133.34, 113.65, 110.78, 31.87, 30.49, 29.28, 29.27, 29.18, 28.72, 22.70, 14.16. HRMS (ESI): m/z $[M + Na]^+$ calcd for $C_{26}H_{36}N_2S_2$: 463.2212; found: 463.2210.

Dimethyl 4-bromophthalate (11): To a 50 mL two-necked round-bottom flask was added 5-bromoisobenzofuran-1,3-dione (0.20 g, 0.88 mmol) and concentrated sulfuric acid (0.090 mL, 1.6 mmol) in methanol (15 mL) under argon. The reaction mixture was heated to reflux for 12 hours, and then cooled to room temperature. After washing with water, the mixture was extracted with DCM, and the organic layers were combined and dried over anhydrous $MgSO_4$. The solid was filtered and the solvent was removed under vacuum. The residue was collected without further purification as a yellow liquid (0.21 g, 0.77 mmol, 87%). The NMR data matched the literature values.[24] ^{1}H NMR ($CDCl_3$, 500 MHz): $\delta = 7.84$ (d, $J = 1.5$ Hz, 1 H), 7.68–7.66 (dd, $J = 2.0$ Hz, 8.5 Hz, 1 H), 7.63 (d, $J = 8.5$ Hz, 1 H), 3.92 (s, 3 H), 3.90 (s, 3 H) ^{13}C NMR ($CDCl_3$, 125 MHz): $\delta = 167.17$, 166.96, 134.19, 134.12, 131.98, 130.70, 130.42, 125.94, 53.09, 52.95 ppm.

5,5'-Bis(tributylstannyl)-2,2'-bithiophene (12): To a 50 mL two-necked round-bottom flask was added 2,2'-bithiophene (0.16 g, 1.0 mmol) and 2.5 molar *n*-BuLi solution (1.0 mL, 2.5 mmol) in THF (10 mL) under argon at −60 °C. The reaction was warmed to 0 °C over 1 hour. After stirring for another 30 minutes and reaching 15 °C, the mixture was cooled to −60 °C and tributyltin chloride (0.98 g, 3.0 mmol) was added. The reaction mixture was stirred overnight and warmed to room temperature gradually. Finally, the reaction was quenched with methanol and the solvent was removed under vacuum. The residue was used for the next step directly without further purification.[67,70] ^{1}H NMR ($CDCl_3$, 500 MHz): $\delta = 7.30$ (d, $J = 3.5$ Hz, 2 H), 7.06 (d, $J = 3.5$ Hz, 2 H), 1.59 (q, $J = 8.0$ Hz, 12 H), 1.36 (sext, $J = 7.5$ Hz, 12 H), 1.12 (t, $J = 8.0$ Hz, 12 H), 0.91 (t, $J = 7.5$ Hz, 18 H). ^{13}C NMR ($CDCl_3$, 125 MHz): $\delta = 143.15$, 136.20, 124.83, 29.11, 27.41, 13.82, 11.01 ppm.

Tetramethyl 4,4'-([2,2'-bithiophene]-5,5'-diyl)diphthalate (PMe-T)$_2$: To a 50 mL two-necked round-bottom flask was added 5,5'-bis(tributylstannyl)-2,2'-bithiophene **12** (0.74 g, 1.0 mmol), dimethyl 4-bromophthalate **11** (0.60 g, 2.2 mmol), and $Pd(PPh_3)_4$ (0.12 g, 0.10 mmol) in degassed toluene (15 mL) under argon. The reaction mixture was stirred at 95 °C for 16 hours. Then the solvent was removed, and the residue was recrystallized from DCM/hexanes to give a bright yellow solid (0.47 g, 0.86 mmol, 86%). ^{1}H NMR ($CDCl_3$, 500 MHz): $\delta = 7.87$ (d, $J = 1.8$ Hz, 2 H), 7.81 (d, $J = 8.1$ Hz, 2 H), 7.73 (d, $J = 8.1$ Hz, 2 H), 7.37 (d, $J = 3.9$ Hz, 2 H), 7.23 (d, $J = 3.9$ Hz, 2 H), 3.95 (s, 6 H), 3.92 (s, 6 H). ^{13}C NMR ($CDCl_3$, 125 MHz): $\delta = 168.33$, 167.26, 141.12, 138.18, 137.13, 133.87, 130.27, 129.62, 127.33, 125.95, 125.48, 125.39, 52.99, 52.81. HRMS (ESI): m/z $[M + H]^+$ calcd for $C_{28}H_{22}O_8S_2$: 551.0829; found: 551.0852.

(3,3'-Dimethyl-[2,2'-bithiophene]-5,5'-diyl)bis(tributylstannane) (14): To a 50 mL two-necked round-bottom flask was added 3,3'-dimethyl-2,2'-bithiophene **4** (70 mg,

0.36 mmol) and 2.5 molar *n*-BuLi solution (0.52 mL, 1.3 mmol) in THF (5 mL) under argon at −60 °C. The reaction mixture was warmed up to 0 °C over 1 hour. After stirring for another 30 minutes and reaching 15 °C, the mixture was cooled to −60 °C and tributyltin chloride (0.35 g, 1.1 mmol) was added. The reaction mixture was warmed to room temperature and stirred overnight. Then the reaction was quenched with methanol and the solvent was removed under vacuum. The residue was used in the next step without further purification.

Tetramethyl 4,4'-(3,3'-dimethyl-[2,2'-bithiophene]-5,5'-diyl)diphthalate (PMe-TMe)$_2$: To a 50 mL two-necked round-bottom flask was added **14** (56 mg, 0.72 mmol), dimethyl 4-bromophthalate **11** (0.43 g, 1.6 mmol), and Pd(PPh_3)$_4$ (82 mg, 0.071 mmol) in degassed toluene (15 mL) under argon. The reaction mixture was stirred at 95 °C for 24 hours. Next, the solvent was removed, and the residue was purified by silica gel chromatography (ethyl acetate) to give a yellow solid (0.21 g, 0.36 mmol, 50%). ^{1}H NMR ($CDCl_3$, 500 MHz): δ = 7.86 (d, J = 1.0 Hz, 2 H), 7.80 (d, J = 8.1 Hz, 2 H), 7.71 (d, J = 9.3 Hz, 2 H), 7.29 (s, 2 H), 3.95 (s, 6 H), 3.92 (s, 6 H), 2.27 (s, 6 H). ^{13}C NMR ($CDCl_3$, 125 MHz): δ = 168.47, 167.45, 141.26, 138.39, 137.41, 133.87, 130.73, 130.30, 129.66, 128.37, 127.42, 125.56, 53.05, 52.88, 15.40. HRMS (ESI): m/z $[M + Na]^+$ calcd for $C_{30}H_{26}O_8S_2Na$: 601.0961; found: 601.0936.

Tributyl(4-octylthiophen-2-yl)stannane (16): To a 25 mL two-necked round-bottom flask was added 3-octylthiophene (0.20 g, 1.0 mmol) and 2.5 molar *n*-BuLi solution (0.48 mL, 1.2 mmol) in THF under argon at −70 °C. After stirring for 1 hour, tributyltin chloride (0.33 g, 1.1 mmol) was added slowly. The reaction mixture was stirred for another 7 hours while warming to room temperature, and then quenched with saturated $NaHCO_3$ solution. The mixture was extracted with DCM, and the organic layers were combined and dried over anhydrous $MgSO_4$. After filtration and evaporation, the residue was used directly without further purification. The NMR matched the literature values.[71] ^{1}H NMR ($CDCl_3$, 500 MHz): δ = 7.21 (s, 1 H), 6.99 (s, 1 H), 2.67 (t, J = 7.5 Hz, 2 H), 1.59–1.55 (m, 12 H), 1.36–1.28 (m, 12 H), 1.11–1.07 (m, 6 H), 0.90 (t, J = 7.5 Hz, 12 H).

Dimethyl 4-(4-octylthiophen-2-yl)phthalate (17): To a 50 mL two-necked round-bottom flask was added dimethyl 4-bromophthalate **11** (0.41 g, 1.5 mmol), tributyl(4-octylthiophen-2-yl) stannane **16** (0.81 g, 1.7 mmol), and Pd(PPh_3)$_4$ (0.17 g, 0.15 mmol) to degassed toluene (10 mL) under argon. The reaction mixture was stirred for 21 hours at 95 °C. After cooling to room temperature, the mixture was poured into water and extracted with DCM, and the organic layers were combined and dried over anhydrous $MgSO_4$. After filtration and evaporation, the residue was purified by silica gel chromatography (ethyl acetate: hexanes = 1/7 to 1/3) to give a yellow liquid (0.57 g, 1.5 mmol, 95%). ^{1}H NMR (DMSO-d_6, 500 MHz): δ = 7.90 (d, J = 1.7 Hz, 1 H), 7.87 (d, J = 8.1 Hz, 1 H), 7.80 (d, J = 8.1 Hz, 1 H), 7.62 (s, 1 H), 7.27 (s, 1 H), 3.84 (s, 3 H), 3.82 (s, 3 H), 2.56 (t, J = 7.6 Hz, 2 H), 1.61–1.58 (m, 2 H), 1.27–1.23 (m, 10 H), 0.84 (t, J = 7.0 Hz, 3 H). ^{13}C NMR ($CDCl_3$, 125 MHz): δ = 168.49, 167.35, 144.88, 141.52, 137.99, 133.74, 130.11, 129.15, 127.37, 126.42, 125.48, 121.62, 52.89, 52.71, 32.00, 30.67, 30.56, 29.54, 29.42, 29.37, 22.79, 14.23. HRMS (ESI): m/z $[M + H]^+$ calcd for $C_{22}H_{29}O_4S$: 389.1781; found: 387.1792.

Dimethyl 4-(5-bromo-4-octylthiophen-2-yl)phthalate (18): To a 15 mL two-necked round-bottom flask was added dimethyl 4-(4-octylthiophen-2-yl)phthalate **17** (55 mg, 0.20 mmol), NBS (39 mg, 0.22 mmol), THF (2 mL), and HOAc (0.5 mL) under argon. The reaction mixture was stirred for 2 hours at 5 °C in the dark. The reaction mixture was purified with silica gel chromatography (ethyl acetate: hexanes = 1/5) to give a yellow liquid (0.070 g, 0.15 mmol, 75%). ^{1}H NMR (CD_3OD, 500 MHz): δ = 7.78 (d, J = 1.7 Hz, 1 H), 7.74 (d, J = 8.1 Hz, 1 H), 7.70 (d, J = 8.1 Hz, 1 H), 7.29 (s, 1 H), 3.90 (s, 3 H), 3.87 (s, 3 H), 2.56 (t, J = 8.0 Hz, 2 H), 1.62–1.59 (m, 2 H), 1.32–1.28 (m, 10 H), 0.88 (t, J = 7.0 Hz, 3 H). ^{13}C NMR (CD_3OD, 125 MHz): δ = 169.53, 168.62, 145.19, 142.31, 138.10, 135.00, 131.19, 130.95, 128.13, 127.49, 125.84, 111.27, 53.33, 53.14, 33.03, 30.72, 30.50, 30.45, 30.37, 30.25, 23.72, 14.46 ppm. HRMS (ESI): m/z $[M + H]^+$ calcd for $C_{22}H_{27}BrO_4S$: 467.0886; found: 467.0897.

Tetramethyl 4,4'-(3,3'-dioctyl-[2,2'-bithiophene]-5,5'-diyl)diphthalate (PMe-Toct)$_2$: To a 15 mL two-necked round-bottom flask was added dimethyl 4-(5-bromo-4-octylthiophen-2-yl)phthalate **18** (0.22 g, 0.47 mmol), bis(1,5-cyclooctadiene) nickel(0) (0.16 g, 0.57 mmol), 2,2′-dipyridyl (88 mg, 0.57 mmol), and THF (4 mL) under argon. The reaction mixture was heated to reflux for 7 hours. After cooling to room temperature, the reaction mixture was purified by silica gel chromatography (hexanes to DCM to ethyl acetate) to give a yellow liquid (0.31 g, 0.39 mmol, 84%). ^{1}H NMR ($CDCl_3$, 500 MHz): δ = 7.87 (d, J = 1.8 Hz, 2 H), 7.81 (d, J = 8.1 Hz, 2 H), 7.72 (d, J = 8.1 Hz, 2 H), 7.32 (s, 2 H), 3.95 (s, 6 H), 3.92 (s, 6 H), 2.56 (t, J = 7.5 Hz, 4 H), 1.63–1.57 (m, 4 H), 1.30–1.21 (m, 20 H), 0.85 (t, J = 7.5 Hz, 6 H) ppm. ^{13}C NMR ($CDCl_3$, 125 MHz): δ = 168.25, 167.12, 144.13, 141.41, 137.27, 133.71, 130.05, 129.73, 129.31, 127.16, 126.63, 125.24, 52.76, 52.58, 31.87, 30.64, 29.39, 29.36, 29.21, 29.07, 22.65, 14.08. HRMS (ESI): m/z $[M + H]^+$ calcd for $C_{44}H_{54}O_8S_2$: 775.3333; found: 775.3324.

6,6'-([2,2'-Bithiophene]-5,5'-diyl)bis(1,3,5-triazine-2,4-diamine) (DAT-T)$_2$: A mixture of **2** (0.10 g, 0.47 mmol), dicyandiamide (0.24 g, 2.8 mmol), and potassium hydroxide (0.060 g, 0.99 mmol) in DMSO (5 mL) was heated at 100 °C overnight. The reaction mixture was cooled and poured into ice cold water. The precipitate that formed was filtered, sonicated in acetone, and heated to reflux in water overnight for further purification to give a yellow solid (0.11 g,

0.29 mmol, 61%). The NMR data matched the literature values.[72] ^{1}H NMR (DMSO-d_6, 300 MHz): δ = 7.76 (s, 2 H), 7.43 (s, 2 H), 6.82 (bs, 8 H). ^{13}C NMR (DMSO-d_6, 125 MHz): δ = 167.42, 166.57, 142.81, 140.18, 130.17, 125.91. HRMS (DART): m/z $[M + H]^+$ calcd for $C_{14}H_{12}N_{10}S_2$: 385.0761; found: 385.0774.

6,6'-(3,3'-Dimethyl-[2,2'-bithiophene]-5,5'-diyl)bis(1,3,5-triazine-2,4-diamine) (DAT-TMe)$_2$: A mixture of **6** (0.10 g, 0.41 mmol), dicyandiamide (0.21 g, 2.5 mmol), and potassium hydroxide (0.050 g, 0.90 mmol) in DMSO (6 mL) was heated at 100 °C for 24 h. The reaction mixture was cooled and poured into ice cold water. The precipitate that formed was filtered, then heated to reflux in water overnight for further purification to give a yellow solid (0.040 g, 0.16 mmol, 40%). ^{1}H NMR (DMSO-d_6, 500 MHz): δ = 7.71 (s, 2 H), 6.78 (bs, 8 H), 2.25 (s, 6 H). ^{13}C NMR (DMSO-d_6, 125 MHz): δ = 166.99, 166.18, 141.72, 136.80, 132.71, 131.98, 15.23. HRMS (ESI): m/z $[M + H]^+$ calcd for $C_{16}H_{16}N_{10}S_2$: 413.1074; found: 413.1078.

Synthesis of 6,6'-(3,3'-Dioctyl-[2,2'-bithiophene]-5,5'-diyl)bis(1,3,5-triazine-2,4-diamine) (DAT-Toct)$_2$: A mixture of **10** (0.11 g, 0.25 mmol), dicyandiamide (0.13 g, 1.5 mmol), and potassium hydroxide (0.034 g, 0.55 mmol) in DMSO (4 mL) was heated at 100 °C for 24 h. The reaction mixture was cooled and poured into ice cold water. The precipitate formed was filtered, sonicated in acetone, and heated to reflux in water overnight for further purification to give a yellow solid (0.089 g, 0.15 mmol, 59%). ^{1}H NMR (DMSO-d_6, 300 MHz): δ = 7.73 (s, 2 H), 6.77 (bs, 8 H), 2.56 (s, 4 H), 1.55–1.47 (m, 4 H), 1.21–1.17 (m, 20 H), 0.80 (t, J = 6.9 Hz, 6 H). ^{13}C NMR (DMSO-d_6, 125 MHz): δ = 167.28, 166.58, 143.11, 142.48, 132.51, 130.87, 31.64, 30.05, 28.88, 28.74, 28.50, 22.42, 14.25. HRMS (ESI): m/z $[M + H]^+$ calcd for $C_{30}H_{44}N_{10}S_2$: 609.3265; found: 609.3257.

5,5'-([2,2'-Bithiophene]-5,5'-diylbis(methanylylidene))bis(pyrimidine-2,4,6(1H,3H,5H)-trione) (B-T)$_2$: A mixture of **1** (0.10 g, 0.45 mmol) and barbituric acid (0.58 g, 4.5 mmol) in ethanol was heated overnight at 70 °C. The reaction mixture was cooled and the precipitate formed was filtered, sonicated in acetone, and heated to reflux in water and ethanol for further purification to give a brown solid (0.18 g, 0.41 mmol, 93%). ^{1}H NMR (DMSO-d_6, 300 MHz): δ = 11.33 (s, 2 H), 8.50 (s, 2 H), 8.20 (d, J = 4.3 Hz, 2 H), 7.84 (d, J = 4.1 Hz, 2 H). HRMS (DART): m/z $[M + H]^+$ calcd for $C_{18}H_{10}N_4O_6S_2$: 443.0115; found: 443.0120.

5,5'-((3,3'-Dimethyl-[2,2'-bithiophene]-5,5'-diyl)bis(methanylylidene))bis(pyrimidine-2,4,6(1H,3H,5H)-trione) (B-TMe)$_2$: A mixture of **5** (0.10 g, 0.45 mmol) and barbituric acid (0.58 g, 4.5 mmol) in ethanol was heated overnight at 70 °C. The reaction mixture was cooled and the precipitate that formed was filtered, sonicated in acetone, and heated to reflux in water and ethanol for further purification to give a brown solid (0.18 g, 0.38 mmol, 93%). ^{1}H NMR (DMSO-d_6, 500 MHz): δ = 11.35 (s, 2 H), 11.32, (s, 2 H) 8.45 (s, 2 H), 8.11 (s, 2 H), 2.31 (s, 6 H). HRMS (ESI): m/z $[M + NH_4]^+$ calcd for $C_{20}H_{14}N_4O_6S_2$: 488.0693; found: 488.0679.

5,5'-((3,3'-Dioctyl-[2,2'-bithiophene]-5,5'-diyl)bis(methanylylidene))bis(pyrimidine-2,4,6(1H,3H,5H)-trione) (B-Toct)$_2$: A mixture of **9** (0.10 g, 0.45 mmol) and barbituric acid (0.58 g, 4.5 mmol) in ethanol was heated overnight at 70 °C. The reaction mixture was cooled and the precipitate that formed was filtered, sonicated in acetone, and heated to reflux in water and ethanol for further purification to give a brown solid (0.18 g, 0.30 mmol, 93%). ^{1}H NMR (DMSO-d_6, 500 MHz): δ = 11.34 (s, 2 H), 11.32 (s, 2 H), 8.49 (s, 2 H), 8.18 (s, 2 H), 2.58 (t, J = 8.0 Hz, 4 H), 1.52–1.57 (m, 4 H), 1.37–1.10 (m, 20 H), 0.80 (t, J = 7.0 Hz, 6 H). ^{13}C NMR (DMSO-d_6, 126 MHz): δ = 163.76, 163.67, 150.65, 147.48, 145.40, 143.43, 143.17, 136.97, 112.71, 31.75, 30.07, 29.02, 29.01, 28.88, 28.31, 22.54, 14.39. HRMS (ESI): m/z $[M + Na]^+$ calcd for $C_{34}H_{42}O_6N_4S_2$: 689.2438; found: 689.2421.

6,6'-([2,2'-Bithiophene]-5,5'-diyl)bis(2,3-dihydrophthalazine-1,4-dione) (PH-T)$_2$: To a 50 mL two-necked round-bottom flask was added tetramethyl 4,4'-([2,2'-bithiophene]-5,5'-diyl) diphthalate **(PMe-T)$_2$** (0.11 g, 0.20 mmol) and hydrazine (0.96 mL, 30 mmol) in anhydrous DMF (10 mL) under argon. The reaction mixture was stirred at 85 °C for 24 hours. Next, the mixture was cooled to 0 °C and methanol (5 mL) was added with stirring. The solid was collected and washed with chloroform and methanol via Soxhlet extraction to give a yellow solid (0.087 g, 0.18 mmol, 90%). ^{1}H NMR (DMSO-d_6, 500 MHz): δ = 8.27 (s, 2 H), 8.20 (d, J = 10.4 Hz, 2 H), 8.12 (d, J = 6.9 Hz, 2 H), 7.79 (b, 2 H), 7.53 (s, 2 H). HRMS (ESI): m/z $[M + H]^+$ calcd for $C_{24}H_{15}N_4O_4S_2$: 485.0384; found: 485.0361.

6,6'-(3,3'-Dimethyl-[2,2'-bithiophene]-5,5'-diyl)bis(2,3-dihydrophthalazine-1,4-dione) (PH-TMe)$_2$: To a 50 mL two-necked round-bottom flask was added tetramethyl 4,4'-(3,3'-dimethyl-[2,2'-bithiophene]-5,5'-diyl) diphthalate **(PMe-TMe)$_2$** (0.10 g, 0.17 mmol) and hydrazine (0.83 g, 26 mmol) in anhydrous DMF (5 mL) under argon. The reaction mixture was stirred at 85 °C for 24 hours. Next, the mixture was cooled to 0 °C and methanol (5 mL) was added with stirring. The solid was collected and washed with chloroform and methanol via Soxhlet extraction to give a yellow solid (0.055 g, 0.11 mmol, 63%). ^{1}H NMR (DMSO-d_6, 500 MHz): δ = 8.25 (s, 2 H), 8.15 (d, J = 8.4 Hz, 2 H), 8.11 (d, J = 8.2 Hz, 2 H), 7.70 (s, 2 H), 2.31 (s, 6 H). HRMS (ESI): m/z $[M + H]^+$ calcd for $C_{26}H_{19}N_4O_4S_2$: 515.0842; found: 515.0863.

6,6'-(3,3'-Dioctyl-[2,2'-bithiophene]-5,5'-diyl)bis(2,3-dihydrophthalazine-1,4-dione) (PH-Toct)$_2$: To a 50 mL two-necked round-bottom flask was added tetramethyl 4,4'-(3,3'-dioctyl-[2,2'-bithiophene]-5,5'-diyl) diphthalate **(PMe-Toct)$_2$** (0.18 g, 0.23 mmol) and hydrazine (1.1 g, 34 mmol) in anhydrous DMF (8 mL) under argon. The reaction mixture was stirred at 85 °C for 24 hours. Then the

mixture was cooled to 0 °C and methanol (5 mL) was added with stirring. The solid was collected and washed with chloroform and methanol via Soxhlet extraction to give a yellow solid (0.14 g, 0.19 mmol, 83%). ^{1}H NMR (DMSO-d_6, 500 MHz): δ = 8.26 (s, 2 H), 8.16 (d, J = 8.3 Hz, 2 H), 8.10 (d, J = 8.3 Hz, 2 H), 7.75 (s, 2 H), 2.62 (t, J = 7.5 Hz, 4 H), 1.68-1.62 (m, 4 H), 1.31-1.20 (m, 20 H), 0.79 (t, J = 6.8 Hz, 6 H). ^{13}C NMR (DMSO-d_6, 125 MHz): δ = 154.98, 154.51, 144.02, 141.38, 136.74, 128.89, 128.80, 128.37, 127.77, 126.29, 126.16, 120.68, 31.29, 29.73, 28.62, 28.44, 22.05, 13.85. HRMS (ESI): m/z $[M + H]^+$ calcd for $C_{40}H_{47}N_4O_4S_2$: 711.3033; found: 711.3033.

Funding Information

R. K. C. and J. X. are thankful to the National Science Foundation for supporting this research (CHE-1507561 and CHE-1904534). The mass spectrometric data were obtained by the UF Department of Chemistry Mass Spectrometry Research and Education Center supported, in part, by the National Institutes of Health (NIH S10OD021758-01A1).

Acknowledgment

C. T. K. wishes to acknowledge the University of Florida (UF) for a Graduate School Fellowship (GSF) which made the preparation of this manuscript possible. We acknowledge the University of Florida Research Computing facilities for providing computational resources and support that have contributed to the research results reported herein (https://www.rc.ufl.edu). We acknowledge the UF Center for Nuclear Magnetic Resonance Spectroscopy for providing necessary instrumentation, equipment, and support that have contributed to these published results.

Supporting Information

Synthesis and structural characterization details, absorption data and associated Beer–Lambert plots, post-deposition analysis by NMR, TGA data, additional STM data, and computational details complete with coordinates of geometry-optimized structures.

Supporting Information for this article is available online at https://doi.org/10.1055/a-1534-1508.

References

(1) Scholz, S.; Kondakov, D.; Lüssem, B.; Leo, K. *Chem. Rev.* **2015**, *115*, 8449.
(2) Wang, C.; Dong, H.; Hu, W.; Liu, Y.; Zhu, D. *Chem. Rev.* **2012**, *112*, 2208.
(3) Li, Y. *Acc. Chem. Res.* **2012**, *45*, 723.
(4) Ostroverkhova, O. *Chem. Rev.* **2016**, *116*, 13279.
(5) Hedley, G. J.; Ruseckas, A.; Samuel, I. D. W. *Chem. Rev.* **2017**, *117*, 796.
(6) Bronstein, H.; Nielsen, C. B.; Schroeder, B. C.; McCulloch, I. *Nat. Rev. Chem.* **2020**, *4*, 66.
(7) Yao, H.; Ye, L.; Zhang, H.; Li, S.; Zhang, S.; Hou, J. *Chem. Rev.* **2016**, *116*, 7397.
(8) Dou, L.; Liu, Y.; Hong, Z.; Li, G.; Yang, Y. *Chem. Rev.* **2015**, *115*, 12633.
(9) Du, Z.; Chen, W.; Chen, Y.; Qiao, S.; Bao, X.; Wen, S.; Sun, M.; Han, L.; Yang, R. *J. Mater. Chem. A* **2014**, *2*, 15904.
(10) Ge, C.-W.; Mei, C.-Y.; Ling, J.; Zhao, F.-G.; Li, H.-J.; Liang, L.; Wang, J.-T.; Yu, J.-C.; Shao, W.; Xie, Y.-S.; Li, W.-S. *J. Polym. Sci., Part A: Polym. Chem.* **2014**, *52*, 2356.
(11) Sun, M.-J.; Zhang, X.; Zhong, Y.-W.; Zhan, C.; Yao, J. *Inorg. Chem.* **2016**, *55*, 13007.
(12) Stupp, S. I.; Palmer, L. C. *Chem. Mater.* **2014**, *26*, 507.
(13) Stebe, K. J.; Lewandowski, E.; Ghosh, M. *Science* **2009**, *325*, 159.
(14) Li, W.; Worfolk, B. J.; Li, P.; Hauger, T. C.; Harris, K. D.; Buriak, J. M. *J. Mater. Chem.* **2012**, *22*, 11354.
(15) Grand, C.; Zajaczkowski, W.; Deb, N.; Lo, C. K.; Hernandez, J. L.; Bucknall, D. G.; Müllen, K.; Pisula, W.; Reynolds, J. R. *ACS Appl. Mater. Interfaces* **2017**, *9*, 13357.
(16) Beaujuge, P. M.; Fréchet, J. M. J. *J. Am. Chem. Soc.* **2011**, *133*, 20009.
(17) Lee, J. K.; Ma, W. L.; Brabec, C. J.; Yuen, J.; Moon, J. S.; Kim, J. Y.; Lee, K.; Bazan, G. C.; Heeger, A. J. *J. Am. Chem. Soc.* **2008**, *130*, 3619.
(18) Li, W.; Zhang, X.; Zhang, X.; Yao, J.; Zhan, C. *ACS Appl. Mater. Interfaces* **2017**, *9*, 1446.
(19) Zhang, T.; Han, H.; Zou, Y.; Lee, Y.-C.; Oshima, H.; Wong, K.-T.; Holmes, R. J. *ACS Appl. Mater. Interfaces* **2017**, *9*, 25418.
(20) Yu, R.; Yao, H.; Hong, L.; Qin, Y.; Zhu, J.; Cui, Y.; Li, S.; Hou, J. *Nat. Commun.* **2018**, *9*, 4645.
(21) Lam, K. H.; Foong, T. R. B.; Ooi, Z. E.; Zhang, J.; Grimsdale, A. C.; Lam, Y. M. *ACS Appl. Mater. Interfaces* **2013**, *5*, 13265.
(22) Aytun, T.; Barreda, L.; Ruiz-Carretero, A.; Lehrman, J. A.; Stupp, S. I. *Chem. Mater.* **2015**, *27*, 1201.
(23) Ouchi, H.; Lin, X.; Kizaki, T.; Prabhu, D. D.; Silly, F.; Kajitani, T.; Fukushima, T.; Nakayama, K.; Yagai, S. *Chem. Commun.* **2016**, *52*, 7874.
(24) Schulze, B. M.; Shewmon, N. T.; Zhang, J.; Watkins, D. L.; Mudrick, J. P.; Cao, W.; Bou Zerdan, R.; Quartararo, A. J.; Ghiviriga, I.; Xue, J.; Castellano, R. K. *J. Mater. Chem. A* **2014**, *2*, 1541.
(25) Shewmon, N. T.; Watkins, D. L.; Galindo, J. F.; Zerdan, R. B.; Chen, J.; Keum, J.; Roitberg, A. E.; Xue, J.; Castellano, R. K. *Adv. Funct. Mater.* **2015**, *25*, 5166.
(26) Zhao, X.; Watkins, D. L.; Galindo, J. F.; Shewmon, N. T.; Roitberg, A. E.; Xue, J.; Castellano, R. K.; Perry, S. S. *Org. Electron.* **2015**, *19*, 61.
(27) Xiao, Z.; Duan, T.; Chen, H.; Sun, K.; Lu, S. *Sol. Energy Mater. Sol. Cells* **2018**, *182*, 1.
(28) Ghosh, T.Panicker, J. S.; Nair, V. C. *Polymers* **2017**, *9*, 112.
(29) Wang, B.; Lin, R.-B.; Zhang, Z.; Xiang, S.; Chen, B. *J. Am. Chem. Soc.* **2020**, *142*, 14399.
(30) Özen, B.; Fadaei Tirani, F.; Schenk, K.; Lin, K.-H.; Scopelliti, R.; Corminboeuf, C.; Frauenrath, H. *Chem. Eur. J.* **2021**, *27*, 3348.
(31) Mayoral, M. J.; Bilbao, N.; González-Rodríguez, D. *ChemistryOpen* **2015**, *5*, 10.

(32) Schulze, B. M.; Watkins, D. L.; Zhang, J.; Ghiviriga, I.; Castellano, R. K. *Org. Biomol. Chem.* **2014**, *12*, 7932.
(33) Geng, K.; He, T.; Liu, R.; Dalapati, S.; Tan, K. T.; Li, Z.; Tao, S.; Gong, Y.; Jiang, Q.; Jiang, D. *Chem. Rev.* **2020**, *120*, 8814.
(34) Luo, J.; Wang, J.-W.; Zhang, J.-H.; Lai, S.; Zhong, D.-C. *CrystEngComm* **2018**, *20*, 5884.
(35) Maly, K. E.; Dauphin, C.; Wuest, J. D. *J. Mater. Chem.* **2006**, *16*, 4695.
(36) Helzy, F.; Maris, T.; Wuest, J. D. *J. Org. Chem.* **2016**, *81*, 3076.
(37) Demers, E.; Maris, T.; Wuest, J. D. *Cryst. Growth Des.* **2005**, *5*, 1227.
(38) Brunet, P.; Simard, M.; Wuest, J. D. *J. Am. Chem. Soc.* **1997**, *119*, 2737.
(39) Deans, R.; Cooke, G.; Rotello, V. M. *J. Org. Chem.* **1997**, *62*, 836.
(40) Miura, A.; Jonkheijm, P.; De Feyter, S.; Schenning, A. P. H. J.; Meijer, E. W.; De Schryver, F. C. *Small* **2005**, *1*, 131.
(41) Yang, W.; Yang, F.; Hu, T.-L.; King, S. C.; Wang, H.; Wu, H.; Zhou, W.; Li, J.-R.; Arman, H. D.; Chen, B. *Cryst. Growth Des.* **2016**, *16*, 5831.
(42) Hollamby, M. J.; Aratsu, K.; Pauw, B. R.; Rogers, S. E.; Smith, A. J.; Yamauchi, M.; Lin, X.; Yagai, S. *Angew. Chem. Int. Ed.* **2016**, *55*, 9890.
(43) Prabhu, D. D.; Aratsu, K.; Yamauchi, M.; Lin, X.; Adhikari, B.; Yagai, S. *Polym. J.* **2017**, *49*, 189.
(44) Yagai, S.; Goto, Y.; Karatsu, T.; Kitamura, A.; Kikkawa, Y. *Chem. Eur. J.* **2011**, *17*, 13657.
(45) Yagai, S.; Goto, Y.; Lin, X.; Karatsu, T.; Kitamura, A.; Kuzuhara, D.; Yamada, H.; Kikkawa, Y.; Saeki, A.; Seki, S. *Angew. Chem. Int. Ed.* **2012**, *51*, 6643.
(46) Yagai, S.; Suzuki, M.; Lin, X.; Gushiken, M.; Noguchi, T.; Karatsu, T.; Kitamura, A.; Saeki, A.; Seki, S.; Kikkawa, Y.; Tani, Y.; Nakayama, K. *Chem. Eur. J.* **2014**, *20*, 16128.
(47) Ouchi, H.; Kizaki, T.; Lin, X.; Prabhu, D. D.; Hoshi, N.; Silly, F.; Nakayama, K.-i.; Yagai, S. *Chem. Lett.* **2017**, *46*, 1102.
(48) Suárez, M.; Lehn, J.-M.; Zimmerman, S. C.; Skoulios, A.; Heinrich, B. *J. Am. Chem. Soc.* **1998**, *120*, 9526.
(49) Kaseyama, T.; Furumi, S.; Zhang, X.; Tanaka, K.; Takeuchi, M. *Angew. Chem. Int. Ed.* **2011**, *50*, 3684.
(50) Mourran, A.; Ziener, U.; Möller, M.; Suarez, M.; Lehn, J.-M. *Langmuir* **2006**, *22*, 7579.
(51) Liu, Y.; Wan, X.; Wang, F.; Zhou, J.; Long, G.; Tian, J.; Chen, Y. *Adv. Mater.* **2011**, *23*, 5387.
(52) Capodilupo, A. L.; De Marco, L.; Fabiano, E.; Giannuzzi, R.; Scrascia, A.; Carlucci, C.; Corrente, G. A.; Cipolla, M. P.; Gigli, G.; Ciccarella, G. *J. Mater. Chem. A* **2014**, *2*, 14181.
(53) Zhuang, W.; Bolognesi, M.; Seri, M.; Henriksson, P.; Gedefaw, D.; Kroon, R.; Jarvid, M.; Lundin, A.; Wang, E.; Muccini, M.; Andersson, M. R. *Macromolecules* **2013**, *46*, 8488.
(54) Stagni, S.; Palazzi, A.; Brulatti, P.; Salmi, M.; Muzzioli, S.; Zacchini, S.; Marcaccio, M.; Paolucci, F. *Eur. J. Inorg. Chem.* **2010**, *2010*, 4643.
(55) Speros, J. C.; Martinez, H.; Paulsen, B. D.; White, S. P.; Bonifas, A. D.; Goff, P. C.; Frisbie, C. D.; Hillmyer, M. A. *Macromolecules* **2013**, *46*, 5184.
(56) Yamamoto, E.; Ukigai, S.; Ito, H. *Chem. Sci.* **2015**, *6*, 2943.
(57) Frisch, G. W. T. M. J.; Schlegel, H. B.; Scuseria, G. E.; Robb, J. R. C. M. A.; Scalmani, G.; Barone, V.; Mennucci, B.; Petersson, H. N. G. A.; Caricato, M.; Li, X.; Hratchian, H. P.; Izmaylov, J. B. A. F.; Zheng, G.; Sonnenberg, J. L.; Hada, M.; Ehara, K. T. M.; Fukuda, R.; Hasegawa, J.; Ishida, M.; Nakajima, T.; Honda, O. K. Y.; Nakai, H.; Vreven, T.; Montgomery, J. A. Jr.; Peralta, F. O. J. E.; Bearpark, M.; Heyd, J. J.; Brothers, E.; Kudin, V. N. S. K. N.; Keith, T.; Kobayashi, R.; Normand, J.; Raghavachari, A. R. K.; Burant, J. C.; Iyengar, S. S.; Tomasi, J.; Cossi, N. R. M.; Millam, J. M.; Klene, M.; Knox, J. E.; Cross, J. B.; Bakken, C. A. V.; Jaramillo, J.; Gomperts, R.; Stratmann, R. E.; Yazyev, A. J. A. O.; Cammi, R.; Pomelli, C.; Ochterski, J. W.; Martin, K. M. R. L.; Zakrzewski, V. G.; Voth, G. A.; Salvador, J. J. D. P.; Dapprich, S.; Daniels, A. D.; Farkas, J. B. F. O.; Ortiz, J. V.; Cioslowski, J.; Fox, A. D. J. Gaussian 09, Revision D.01. Wallingford CT: Gaussian, Inc.; **2013**.
(58) Kale, T. S.; Ardoña, H. A. M.; Ertel, A.; Tovar, J. D. *Langmuir* **2019**, *35*, 2270.
(59) Barbarella, G.; Zambianchi, M.; Bongini, A.; Antolini, L. *Adv. Mater.* **1993**, *5*, 834.
(60) Fitzner, R.; Reinold, E.; Mishra, A.; Mena-Osteritz, E.; Ziehlke, H.; Körner, C.; Leo, K.; Riede, M.; Weil, M.; Tsaryova, O.; Weiß, A.; Uhrich, C.; Pfeiffer, M.; Bäuerle, P. *Adv. Funct. Mater.* **2011**, *21*, 897.
(61) Grell, M.; Bradley, D. D. C.; Ungar, G.; Hill, J.; Whitehead, K. S. *Macromolecules* **1999**, *32*, 5810.
(62) Steinberger, S.; Mishra, A.; Reinold, E.; Levichkov, J.; Uhrich, C.; Pfeiffer, M.; Bäuerle, P. *Chem. Commun.* **2011**, *47*, 1982.
(63) Zhou, N.; Guo, X.; Ortiz, R. P.; Li, S.; Zhang, S.; Chang, R. P. H.; Facchetti, A.; Marks, T. J. *Adv. Mater.* **2012**, *24*, 2242.
(64) Lee, J.-I.; Lee, V. Y.; Miller, R. D. *ETRI J.* **2002**, *24*, 409.
(65) Katsonis, N.; Xu, H.; Haak, R. M.; Kudernac, T.; Tomović, Ž.; George, S.; Van der Auweraer, M.; Schenning, A. P. H. J.; Meijer, E. W.; Feringa, B. L.; De Feyter, S. *Angew. Chem. Int. Ed.* **2008**, *47*, 4997.
(66) Cañas-Ventura, M. E.; Aït-Mansour, K.; Ruffieux, P.; Rieger, R.; Müllen, K.; Brune, H.; Fasel, R. *ACS Nano* **2011**, *5*, 457.
(67) Pandolfi, F.; Rocco, D.; Mattiello, L. *Org. Biomol. Chem.* **2019**, *17*, 3018.
(68) Shinde, V. N.; Bhuvanesh, N.; Kumar, A.; Joshi, H. *Organometallics* **2020**, *39*, 324.
(69) Maior, R. M. S.; Hinkelmann, K.; Eckert, H.; Wudl, F. *Macromolecules* **1990**, *23*, 1268.
(70) J.-A. K. Hong, Ran; Yun, Hui-Jun; Park, Joung-Man; Shin, Sung Chul; Kim, Yun-Hi *Bull. Korean Chem. Soc.* **2013**, *34*, 1170.
(71) Chen, L. X.; Xiao, S.; Yu, L. *J. Phys. Chem. B* **2006**, *110*, 11730.
(72) Rodrigues, A. D.; Marcotte, N.; Quignard, F.; Deabate, S.; Robitzer, M.; Lerner, D. A. *Spectrochim. Acta, Part A* **2020**, *227*, 117708.